2005 WSEAS Int. Conf. on DYNAMICAL SYSTEMS and CONTROL, Venice, Italy, November 2-4, 2005 (pp385-390)

Design of Resonant Controllers for Current Control Loop by using the Causal Ordering Graph - Application to Machine Tools -

Ghislain REMY, Julien GOMAND, Pierre-Jean BARRE, Jean-Paul HAUTIER
Laboratory of Power Electronics and Electrical Engineering of Lille (L2EP)
Technological Research Team – ERT CEMODYNE
ENSAM, 8 Bd Louis XIV, 59046 Lille Cedex
FRANCE
http://www.lille.ensam.fr/cemodyne

Abstract: - Industrial computer numerical controllers (CNC) in machine tools applications are classically composed of three cascaded closed loops: current, speed and position loop, from internal to external loop in that order. Typically, IP controllers are used in the closed current control loop. In order to increase the precision of such system, we propose to design for the current loop a new controller by using resonant controllers. Today, machine tools actuators are made with linear drives, mainly with permanent magnet linear synchronous motors (PMLSM). We present a model of PMLSM including harmonics of Back Electromotive Force (EMF) using the Causal Ordering Graph (COG). Then, we propose the design of resonant controllers for the current control loop by using the inversion principle of the COG. Experimental results are shown to improve the effectiveness of resonant controllers.

Key-Words: - Resonant Controllers, Current Control Loop, Causal Ordering Graph, Machine Tools, PMLSM

1 Introduction

Nowadays, the machine tools framework use linear drives for high performances: high traverse speeds, very high acceleration due to their low inertia, high reliability due to a small number of components, reduced bulk, which facilitates the construction of compact machines [1]. The linear motor used is principally an iron core, single side, flat permanent magnet linear synchronous motor (PMLSM) [2]. Such linear drives are controlled with industrial computer numerical controllers (CNC) generally composed of three cascaded closed loop: from the internal to the external closed loops, we find an IP controller for the current control loop, an IP controller for the speed control loop and finally a P controller for the position control loop, Fig.1 [3].

The field-oriented control with IP controllers for the current control loop in synchronous d-q reference frame is used to control such systems. Nevertheless, that controller is only adapted to compensate a constant error generated between reference and measure currents. But it has been shown that sinusoidal error in the current measure cannot be compensated with an IP controller [4]. Non sinusoidal EMF will create harmonics on current and undesired ripples in the thrust [5].

In order to improve the performance of such systems, we propose to design a current control loop with new controllers based on resonant controllers. First, we model the current control loop of the actuator using the Causal Ordering Graph representation [6]. Then, with the inversion principle of the COG [7], we propose a new design of the current control loop with a resonant controller. Finally, experimental results show the effectiveness of the method.

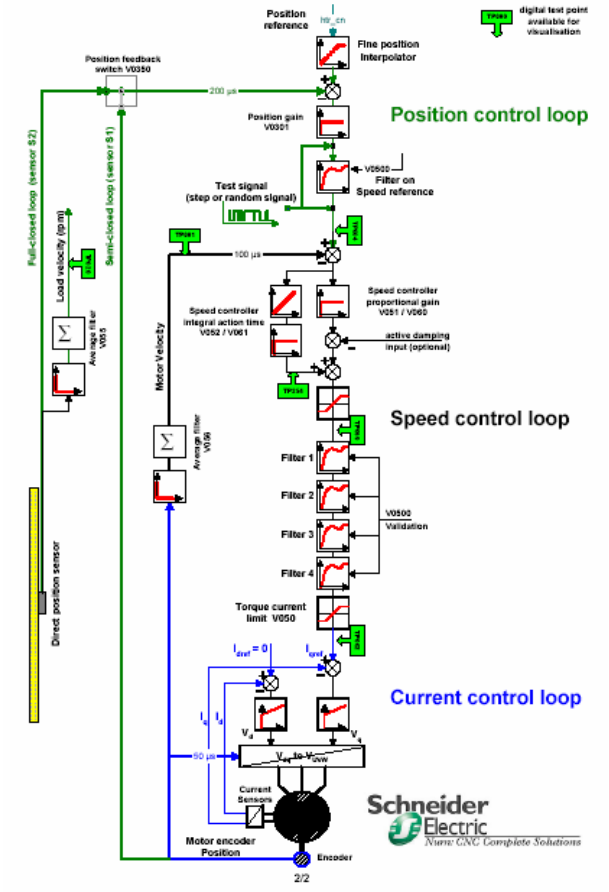

Fig.1: Structure of the Num CNC (Schneider) [3].

2 Causal Model of a Linear Drive

2.1 Model of PMLSM

In this section, we present the model of a PMLSM with a non-sinusoidal back EMF. To adapt the proposed control structure, this model is established in the Concordia reference frame, Fig.2.

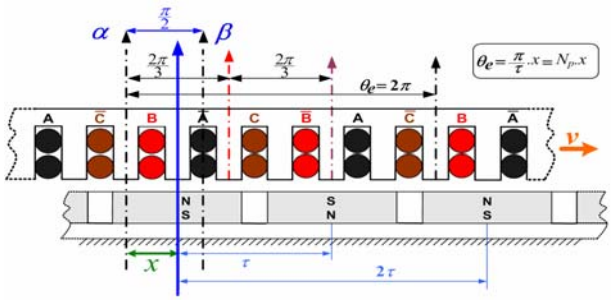

Fig.2: Principle schematic of a PMLSM

Then, the voltage equations of the PMLSM in the Concordia reference frame can be expressed as:

$$[V_{\alpha\beta}] = \left([R] + \frac{d[L_{\alpha\beta}]}{dt}\right)\cdot[i_{\alpha\beta}] + [L_{\alpha\beta}]\cdot\frac{d[i_{\alpha\beta}]}{dt} + \sqrt{\frac{3}{2}}\cdot N_p v\hat{\phi}_f \cdot \sum_{n=1}^{\infty}\lambda_{2n-1}\cdot\begin{bmatrix}\lambda_{\alpha}^{2n-1}\cdot\sin[(2n-1)\theta]\\ \lambda_{\beta}^{2n-1}\cdot\cos[(2n-1)\theta]\end{bmatrix} \quad (1)$$

Wherein $\hat{\phi}_f$ denotes the maximum value of magnetic excitation flux per phase in a natural a-b-c reference frame. The inductance matrix is given by:

$$[L_{\alpha\beta}] = \begin{bmatrix} L_s - M_s & 0 \\ 0 & L_s - M_s \end{bmatrix} \quad (2)$$

The electromagnetic thrust generated by the PMLSM is created by the interaction between the winding currents and the permanent magnetic field. It may be expressed as:

$$T_e = \sqrt{\frac{3}{2}}\cdot N_p\hat{\phi}_f\cdot[i_\alpha\ i_\beta]\cdot \begin{bmatrix} -\sum_{n=0}^{\infty}\{\lambda_{6n+1}\cdot\sin[(6n+1)\theta]\} - \sum_{n=1}^{\infty}\{\lambda_{6n-1}\cdot\sin[(6n-1)\theta]\} \\ \sum_{n=0}^{\infty}\{\lambda_{6n+1}\cdot\cos[(6n+1)\theta]\} - \sum_{n=1}^{\infty}\{\lambda_{6n-1}\cdot\cos[(6n-1)\theta]\} \end{bmatrix} \quad (3)$$

2.1.1 The Causal Ordering Graph

The Causal Ordering Graph is built up with several graphical processors attached to different objects located in the studied process. As seen in the previous section, the evolution of these objects is characterized by a transformation relation between influencing quantities and influenced quantities. This relation is induced by the principle of causality governing the energetic relation of an object or group of objects. In short, the output of a processor only depends on present or past values of the inputs. Such a formulation expresses the causality in integral form and there are many significant electrical and mechanical examples which illustrate this concept. Since the flux in a self is an integral function of the voltage, by analogy, the kinetic moment of a rigid mass is the integral function of the applied efforts. The electricity quantity in a capacitor is an integral function of the current; by analogy, the endpoints position of a spring is the integral of the velocity variation between the endpoints (Hooke's law).

In general, the expression of the transformation relations by means of the state equations is the best warranty against physical misinterpretation. To simplify the presentation, we will only retain two complementary definitions of the integral causality: (a) If an object accumulates information, causality is internal: the output is necessarily a function of the energy state, the relation then oriented is known as causal. Time and the initial state are implicit inputs and are not represented. (b) If an object does not accumulate information, causality is external. The output is an instantaneous function of the input. The relation, which is not oriented, is then known as rigid. Fig.3 gives the selected symbolism to differentiate the two kinds of processors.

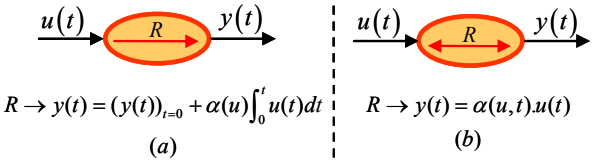

Fig.3: COG symbolisms:
(a) causal relation, (b) rigid relation.

2.1.2 Application of the COG to a PLMSM model

By applying the previous rules, the COG representation of the PMLSM model is illustrated in Fig.4. The model presented shown only the electrical phenomena of the PMLSM that needed to be taken into account for the current control loop.

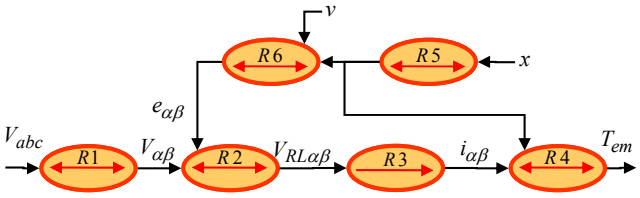

Fig.4: COG of the PMLSM model

The different relations are given by:

$$R2 \rightarrow V_{RL\alpha} = V_\alpha + e_\alpha,\ R6 \rightarrow e_\alpha = v\cdot N_p\cdot\frac{d\phi_\alpha}{dx}$$

$$R3 \rightarrow \left(R + L_\alpha\cdot\frac{d}{dt}\right)\cdot i_\alpha = V_{RL\alpha}$$

$$R4 \rightarrow T_{em} = i_\alpha\cdot\frac{d\phi_\alpha}{dx} + i_\beta\cdot\frac{d\phi_\beta}{dx}$$

$$R5 \rightarrow \frac{d\phi_{\alpha\beta}}{dx} = \sqrt{\frac{3}{2}} \cdot N_p \cdot \hat{\phi}_f \sum_{n=1}^{\infty} \begin{bmatrix} \lambda_\alpha^{2n-1} \cdot \sin\left[(2n-1) N_p \cdot x\right] \\ \lambda_\beta^{2n-1} \cdot \cos\left[(2n-1) N_p \cdot x\right] \end{bmatrix}$$

2.2 Harmonics of Electromotive Force

The studied PMLSM is a Rexroth LSP120C linear motor. The coefficients λ_α^{2n-1}, λ_β^{2n-1} of EMF harmonics are experimentally identified (1) and are listed in Table 1 [9].

Table 1: Coefficients of Electromotive Force harmonics

Coefficient names	λ_1	λ_5	λ_7	λ_{11}
Coefficient values	1	-0.0267	0.000423	0.000459

If we neglect the effects of EMF harmonics, the waveforms of currents i_α and i_β should be sinusoidal. By substituting these coefficients into (3), we can notice that thrust ripples will be introduced by non-sinusoidal EMF. The thrust ripple caused by the 5th EMF harmonic could reach 2.67%, which is the dominant ripple source. However, those caused by the 7th and 11th harmonics are so slight (0.1% in total) that their influence can be neglected.

3 Controller synthesis by inverse model

3.1 Inversion Principle of COG

The process model is now used to deduce the control structure by using the inversion principle. Rigid processors can be directly inverted:

$$\begin{aligned} &R \rightarrow y = R(u), \quad R_c \rightarrow u_{reg} = C(y_{ref}) \\ &IF \;\; u = u_{reg} \;\text{ AND }\; C = R^{-1}, \;\text{ THEN }\; y = y_{ref} \end{aligned} \tag{4}$$

Causal processors call for an indirect inversion (control loop):

$$\begin{aligned} &R \rightarrow y = R(u), \quad R_c \rightarrow u_{reg} = C(y_{ref} - \hat{y}) \\ &IF \;\; u = u_{reg} \;\text{ AND }\; C \rightarrow \infty, \;\text{ THEN }\; y \rightarrow y_{ref} \end{aligned} \tag{5}$$

These causal and rigid inversions are presented in Fig.5:

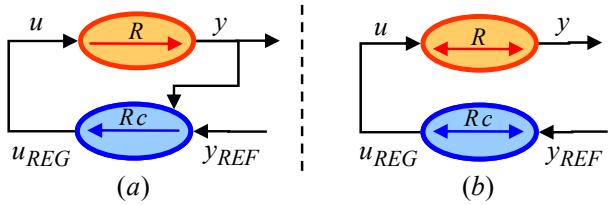

Fig.5: Inversion Principle of the COG: (a) causal relation, (b) rigid relation.

3.2 Controller Synthesis

If we apply the inversion principle on our PMLSM model, we obtain this controller design, Fig.6:

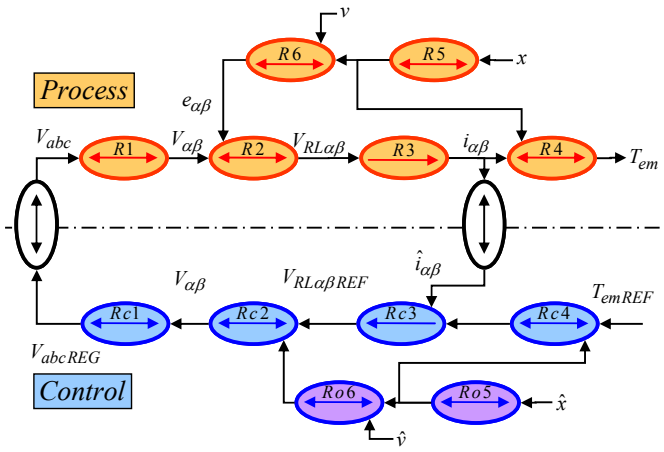

Fig.6: PMLSM thrust control scheme

The different relations are given by:

$$Rc2 \rightarrow V_{\alpha ref} = V_{RL\alpha ref} - \tilde{e}_\alpha$$

$$Rc3 \rightarrow V_{RL\alpha REF} = C_\alpha (i_{\alpha ref} - \hat{i}_\alpha)$$

$$Rc4 \rightarrow \begin{cases} i_{\alpha ref} = \dfrac{T_{emREF} \cdot \left[-\sin(N_p \hat{x}) + \lambda_5 \cdot \sin(5 N_p \hat{x})\right]}{\sqrt{\frac{3}{2}} \cdot N_p \cdot \hat{\phi}_f \cdot (1 - \lambda_5^2)} \\ i_{\beta ref} = \dfrac{T_{emREF} \cdot \left[\cos(N_p \hat{x}) + \lambda_5 \cdot \cos(5 N_p \hat{x})\right]}{\sqrt{\frac{3}{2}} \cdot N_p \cdot \hat{\phi}_f \cdot (1 - \lambda_5^2)} \end{cases}$$

$$Ro5 \rightarrow \frac{d\tilde{\phi}_\alpha}{dx} = \sqrt{\frac{3}{2}} \cdot N_p \cdot \hat{\phi}_f \sum_{n=1}^{\infty} \begin{bmatrix} \lambda_\alpha^{2n-1} \cdot \sin\left[(2n-1) N_p \cdot \hat{x}\right] \\ \lambda_\beta^{2n-1} \cdot \cos\left[(2n-1) N_p \cdot \hat{x}\right] \end{bmatrix}$$

$$Ro6 \rightarrow \tilde{e}_\alpha = \hat{v} \cdot N_p \cdot \frac{d\tilde{\phi}_\alpha}{dx}$$

The three-phase load currents are measured, transformed and regulated by two controllers in the Concordia reference frame. The mover position is detected and fed into the block of "Excitation Currents Generator" to generate instantaneous thrust command. The angular speed ω is estimated and fed into the controllers so that they can adapt to the reference currents with time-varying frequency.

4 Resonant controller

Given our model of Back EMF, composed of harmonics (Table 1), we have decided to compensate two harmonics of Back-EMF: the fundamental and the 5th harmonic. Thus, the resonant controllers have identical

structures with two resonant frequencies. In this way, the tracking of the reference currents and the rejection of disturbances from non-sinusoidal back-EMF can be simultaneously realised.

The general transfer function of a multiple-frequency resonant controller is given by:

$$C(s)=\frac{\sum_{j=0}^{2k} b_j s^j}{\prod_{i=1}^{k}\left(s^2+\omega_i^2\right)} \qquad (6)$$

Wherein k denotes the number of associated resonant elements and ω_i correspond to the concerned resonant frequencies.

The Bode diagrams of the open-loop transfer function of the control system using a two-frequency resonant controller can be seen in Fig.7. We can note that infinite gains are produced at the concerned frequencies (ω_0, $5\omega_0$), which ensures that the steady-state error at these frequencies can be completely eliminated.

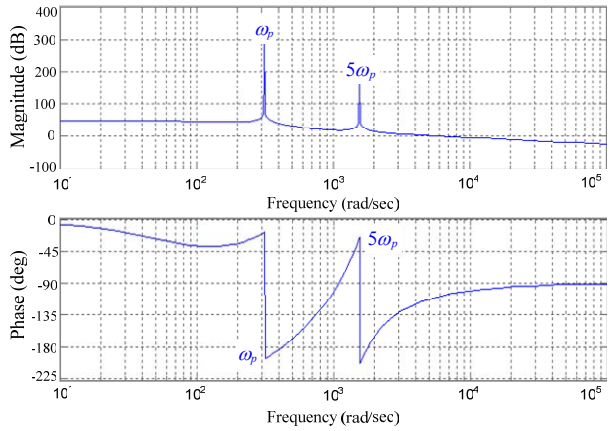

Fig.7: Bode diagram of open-loop transfer function

The coefficients of controller can be determined by using the pole assignment technique [10]: All poles of the closed-loop system will be placed on a vertical line in the pole-zero map, as shown in Fig.8 [11]. Then, we choose to control all system zeros around another vertical line, therefore minimizing their influences on system stability.

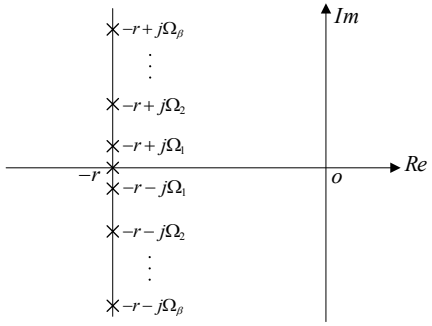

Fig.8: Bode diagram of open-loop transfer function

5 Experimental results

The proposed approach is experimentally verified on a laboratory test system equipped with a Rexroth LSP120C linear motor, Fig.9. Table 2 lists the specifications of the test system. The control scheme depicted in Fig.8 is implemented in a dSPACE DS1005 real-time digital control card to drive the PMLSM through an IGBT inverter. We have used a Heidenhain exposed linear encoder with a grating period of 20μm, which is a high precision incremental encoder, to detect the mover position.

Fig.9: Linear Motor Rexroth LSP120C

Table 2: The test system: specifications and parameters

Specifications		Parameter Value
PMLSM	Inductance	$L_s = 16.2[mH]$
	Resistance	$R_s = 1.1[\Omega]$
	Max value of magnet excitation flux / phase	$\hat{\phi}_f = 0.65[Wb]$
	Pole pitch	$\tau = 37.5[mm]$
	Electrical position constant	$N_p = 83.8[mm^{-1}]$
	Mass of mobile part	$M = 200[kg]$
Switching Frequency of IGBT		10 [kHz]

The experimental references, measurements and estimations of currents and thrust are presented for a current control system using an IP controller, Fig.10 and for an AC current control system using two-frequency resonant controllers, Fig.11.

The reference thrust has a trapezoidal waveform defined with a jerk maximum value of 1500m/s^3 and with an acceleration value of 7.5m/s^2. The jerk value is needed to hold the measurement tracking of the incremental position sensor. This reduces the probability of having a tracking error.

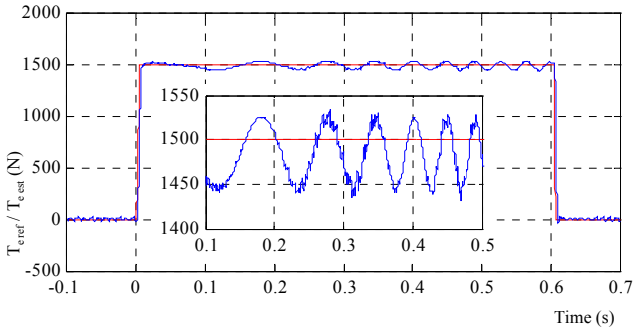

Fig.10: current control system using IP controllers

As noticed in (3), the harmonics of Back EMF induced harmonics of currents. Consequently, ripple forces on the thrust with an IP controller could not be eliminated, Fig.10. The IP controller is designed in order to compensate the predominating pole of the linear motor. Classically, this pole is based on the electrical time constant.

In the Concordia reference frame, we verify that currents have a sinusoidal waveform, the frequency of which increases with the speed of the linear motor Fig.11.

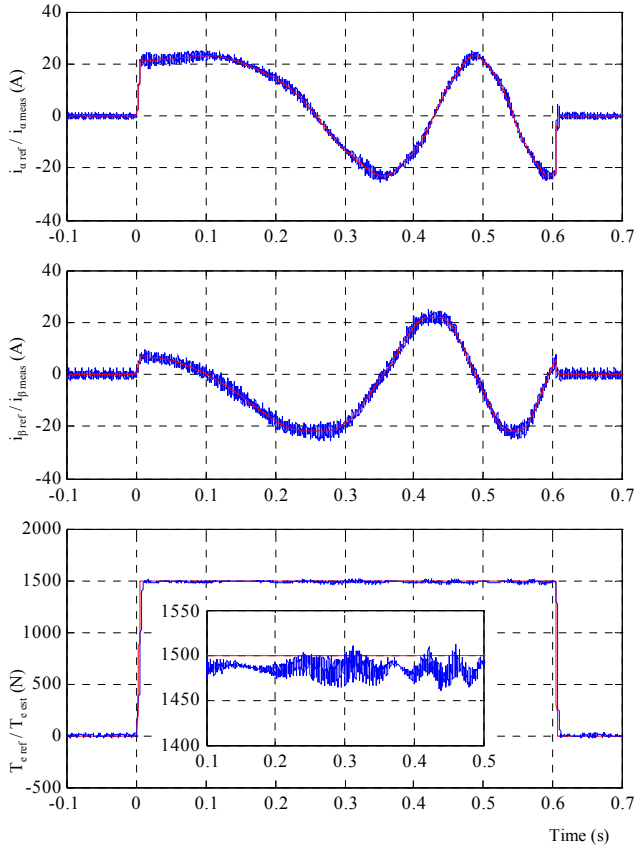

Fig.11: AC current control system using two-frequency resonant controllers

With an AC current control system using two-frequency resonant controllers, results are notable. Indeed, the load currents are very close to their references. The maximal delay of the load currents stays under 0.5ms, even if brutal changes occur in current references. When the non-sinusoidal EMF is not compensated (3), we notice a ripple of 5% on thrust estimation. After the compensation using two-frequency resonant controllers, the ripple is reduced to 1% of the estimated thrust.

The measurement thrust on Fig.11 has some residual ripple caused by the 7th harmonics and higher rank of the Back-EMF.

Nevertheless, the load current is noisy, because we need to inject the measure of the 5th harmonic of the currents.

On the results of the thrust, we notice that estimated thrust underrates the value of reference thrust. In fact, with our resonant controllers, Back-EMF compensation isn't needed. Indeed, this error is generally constant and could be compensated by the IP controller of the speed control loop. So it isn't necessary to have a Back-EMF estimator in our control structure.

Mostly, high speed machine tools use linear motors which are designed for high dynamic. As a result the mass and stiffness of the moving part are reduced. The main drawback is that ripple thrusts in Fig.10 aren't compensated by the inertia of the moving part anymore, and so the ripple thrusts have to be compensated by new controllers.

6 Conclusion

This paper has presented a novel approach to improve the thrust control performance of a PMLSM with non-sinusoidal Back-EMF. First, a model of PMLSM with non-sinusoidal Back-EMF is presented with the Causal Ordering Graph representation. Then, by applying the inversion principle of the COG, we have deduced the controller synthesis. Next, a multi-frequency resonant controller is proposed to ensure the tracking of the desired current waveforms. That has allowed us to compensate for the non-sinusoidal Back-EMF. Finally, experimental results are shown from a laboratory test system and verify the effectiveness of the suggested approach. Finally, the ripple of 5% on thrust estimation with an IP controller is reduced to 1% of the estimated thrust with a resonant controller. Future work will present a new speed control loop with a detent force compensation, and will show Back-EMF estimator influences.

References:

[1] J.F. Eastham, A. Tenconi, F. Profumo, G. Gianolio, Linear Drive in Industrial Application: State of the Art and Open Problems, *Proceedings of the International Conference on Electrical Machines* (ICEM'02), Proceedings CD-ROM, Bruges, August 2002.

[2] A. Cassat, N. Corsi, N. Wavre, R. Moser, Direct Linear Drives: Market and Performance Status, *Proceedings of the 4th International Symposium on Linear Drives for Industry Applications* (LDIA2003), Birmingham, UK, Sept. 8-10 2003.

[3] M. Aubourg, Procédures de réglage des axes de machine outils, *Centre Techniques des Industries Mécaniques*, CETIM, CDROM, 2003.

[4] P.J. Barre, A. Tounzi, J.P. Hautier, S. Bouaroudj, Modelling and thrust control using resonating controller of asymmetrical PMLSM, 9th European Conference on Power Electronics and Applications, EPE 2001, Graz, 27-29 August 2001.

[5] G. Remy, A. Tounzi, P.J. Barre, F. Francis, J.P. Hautier, Finite-Element Analysis of Non-Sinusoidal Electromotive Force in a Permanent Magnet Linear Synchronous Motor, *The Fifth International Symposium on Linear Drives for Industry Applications* (LDIA2005), Kobe-Awaji, Japan, Sept. 25-28 2005.

[6] X. Guillaud, P. Degobert, J.P. Hautier, Modeling Control and Causality: The Causal Ordering Graph, *16th IMACS Control Engineering Lausanne* (CD Rom), August 2000.

[7] J.P. Hautier, P.J. Barre, The Causal Ordering Graph A tool for system modelling and control law synthesis, *Journal of studies in informatics and control*, Vol. 13, No. 4, 2004, pp. 265-283.

[8] J. Zeng, P.J. Barre, P. Degobert, Modeling and Thrust Control of PMLSM using Principle of Local Energy, *proceedings of the Sixth International Conference on Electrical Machines and Systems* (ICEMS2003), Beijing, P.R. China, Nov. 9-11 2003.

[9] G. Remy, A. Tounzi, P.J. Barre, F. Francis, J.P. Hautier, Finite-Element Analysis of Non-Sinusoidal Electromotive Force in a Permanent Magnet Linear Synchronous Motor, *The Fifth International Symposium on Linear Drives for Industry Applications*, LDIA2005, Kobe-Awaji, Japan, 25-28 Sept. 2005.

[10] J. Zeng, G. Remy, P. Degobert, P.J. Barre, Thrust Control of the Permanent Magnet Linear Synchronous Motor with Multi-Frequency Resonant Controllers, *in proceeding of the 18th International Conference on Magnetically Levitated Systems and Linear Drives* (Maglev'2004), October, 2004, Shanghai, China, Vol. 2, Page: 886-896.

[11] J. Zeng, P. Degobert, J.P. Hautier, Torque Ripple Minimization in Permanent Magnet Synchronous Motor Drives, *the 6th International Symposium on Advanced Electro Mechanical Motion Systems* (ELECTROMOTION 2005), 27-29, September, 2005, Lausanne, Switzerland.